Homogeneous Ice Nucleation and Supercooled Liquid Water in Orographic Wave Clouds

ANDREW J. HEYMSFIELD AND LARRY M. MILOSHEVICH

National Center for Atmospheric Research, Boulder, Colorado*

(Manuscript received 4 June 1992, in final form 12 October 1992)

ABSTRACT

This study investigates ice nucleation mechanisms in cold lenticular wave clouds, a cloud type characterized by quasi-steady-state air motions and microphysical properties. It is concluded that homogeneous ice nucleation is responsible for the ice production in these clouds at temperatures below about −33°C. The lack of ice nucleation observed above −33°C indicates a dearth of ice-forming nuclei, and hence heterogeneous ice nucleation, in these clouds.

Aircraft measurements in the temperature range −31° to −41°C show the following complement of simultaneous and abrupt changes in cloud properties that indicate a transition from the liquid phase to ice: disappearance of liquid water; decrease in relative humidity from near water saturation to ice saturation; increase in mean particle size; change in particle concentration; and change in temperature due to the release of latent heat. A numerical model of cloud particle growth and homogeneous ice nucleation is used to aid in interpretation of our in situ measurements. The abrupt changes in observed cloud properties compare favorably, both qualitatively and quantitatively, with results from the homogeneous ice nucleation model. It is shown that the homogeneous ice nucleation rates from the measurements are consistent with the temperature-dependent rates employed by the model (within a factor of 10^2, corresponding to about 1°C in temperature) in the temperature range −35° to −38°C. Given the theoretical basis of the modeled rates, it may be reasonable to apply them throughout the −30° to −50°C temperature range considered by the theory.

The absence of convincing liquid water detection in past in situ cloud studies at temperatures below about −36°C is found to be the result of instrument detection thresholds. Evidence that droplets can exist, under liquid-subsaturated conditions, at temperatures at least as low as −40.7°C is presented. The findings are also used to discuss ice production via homogeneous nucleation in cirrus clouds. Relative humidity measurements from a newly developed airborne cryogenic frostpoint hygrometer were found to be reliable and crucial to studies of homogeneous ice nucleation.

1. Introduction

In recent years increasing attention has been focused on mid- and upper-tropospheric ice clouds, through such field campaigns as the First ISCCP Research Experiment (FIRE; Cox et al. 1987) and the International Cirrus Experiment (ICE; Raschke 1988), as the meteorological community has become more aware of the potential importance of these clouds to the radiative properties of the atmosphere and to global climate (e.g., Ramanathan and Collins 1991). The radiative properties of these clouds depend strongly on their microphysical composition, particularly hydrometeor size spectra and shapes (Smith 1990; Wielicki et al. 1990; Stephens et al. 1990), and ice size spectra are strongly influenced by ice production rates and ice nucleation mechanisms. The ice nucleation process therefore indirectly plays an important role in determining the radiative properties of ice clouds, and an understanding of this process is necessary for the proper treatment of cirrus clouds in numerical models.

It is difficult to observationally investigate ice nucleation mechanisms in cirrus, since the conditions when sampled crystals are produced may not be known and instrumentation to measure hydrometeor size distributions, crystal shapes, and relative humidity may be inadequate. In our study, we consider the relatively simple and quasi-steady-state dynamical and microphysical framework of orographically formed lenticular wave clouds to gain an understanding of the ice nucleation process at temperatures below −30°C. Our approach combines in situ measurements and numerical modeling calculations.

Liquid droplets have been detected in situ at temperatures down to about −36°C (e.g., Sassen and Dodd 1988; Heymsfield et al. 1991), where ice nucleation evidently does not readily take place *heterogeneously* on immersion (freezing) or deposition ice nuclei, suggesting that such nuclei are scarce in the upper troposphere or that these ice nucleation mechanisms are

* The National Center for Atmospheric Research (NCAR) is sponsored by the National Science Foundation.

Corresponding author address: Dr. Andrew J. Heymsfield, Meso- and Microscale Meteorology Division, NCAR, P.O. Box 3000, Boulder, CO 80307-3000.

© 1993 American Meteorological Society

slow to operate. As the temperature decreases below about −36°C, if heterogeneous ice nucleation mechanisms are inconsequential, ice nucleation will in theory take place *homogeneously,*[1] without the need for immersion or deposition ice nuclei.

The temperature to which liquid water (LW) can supercool has been a subject of academic interest and controversy over the past 40 years. Hosler and Spalding (1955) and Day (1958) demonstrated in laboratory studies that the probability of homogeneous freezing depended on droplet size and that micron-size water droplets could supercool to about −38°C before freezing. Studies of geyser plumes by Schaefer (1962) indicated a remarkable difference in optical properties of the plumes at temperatures of −36° to −38°C compared with temperatures of −40°C and below, and there was no evidence of supercooled droplets at temperatures below −38°C. These data were used by Schaefer to refute the idea that droplets could supercool to as low as −65°C in thunderstorms, as implied by aircraft icing reports (Simpson 1963). Droplets in naturally occurring clouds form on soluble CCN, which depress the freezing point of the resulting solution droplets relative to pure water by an amount related to the molality of the solution. Heymsfield and Sabin (1989) and Sassen and Dodd (1989) employed numerical modeling studies to quantify the proposal that very small, unactivated solution droplets[2] could supercool well below −40°C. Sassen and Dodd (1988) detected LW in wave clouds at −36°C and deduced the presence of LW at −37°C from ground-based lidar depolarization measurements; however, their use of a sounding to establish a temperature–altitude correlation is unreliable since our wave cloud measurements show that the temperature at a given altitude across a wave cloud may vary by as much as 4°C. DeMott and Rogers (1990) have shown in a laboratory cold room that dilute solution droplets can supercool to about −37°C.

The NCAR Sabreliner and King Air aircraft flew research missions in wave clouds in northern Colorado and southern Wyoming during the fall of 1989 and 1990, in part to test new instrumentation prior to Project FIRE Phase II. The resulting observations are unique in several respects. As will be shown, accurate relative humidity measurements at low temperatures were made possible by a newly developed airborne cryogenic frostpoint hygrometer. The aircraft sampling pattern was conducive to observation and interpretation of the ice nucleation process. In addition, these wave clouds allow estimates of the meteorological conditions experienced by cloud particles from the leading edge of the cloud to the location at which they were sampled.

We explore the following questions in this study:

1) Are the measurements consistent with the freezing of solution droplets through homogeneous ice nucleation?

2) Under what thermodynamic conditions does homogeneous ice nucleation operate, and consequently under what conditions can supercooled liquid water exist?

3) Can we determine homogeneous ice nucleation rates from the measurements?

4) What variables are important in determining the ice particle size spectrum that results from homogeneous ice nucleation?

5) How might the homogeneous ice nucleation mechanism apply to cirrus clouds?

2. Aircraft instrumentation

The measurements to be presented in section 3 employed the NCAR Sabreliner and King Air aircraft, whose performance characteristics and instrumentation are described in detail in RAF Bulletins Nos. 2 and 3 (available from NCAR). Vertical velocity measurements are accurate to better than 1 m s^{-1} in an absolute sense and 25 cm s^{-1} in a relative sense for individual cloud penetrations.

Droplet size distributions were measured in 15 size categories with Particle Measuring Systems (PMS) forward scattering spectrometer probes (FSSP), nominally sizing between 2 and 32 μm or 3 and 45 μm depending on the size range selected. The FSSP data were not corrected for known sizing inaccuracies resulting from airspeed effects and optical properties of the probe (Baumgardner and Spowart 1990); however, accurate particle sizing is not crucial to our arguments. Particle concentrations in this study are used primarily in a relative sense, and effects of ice on FSSP-derived concentrations are discussed in section 3.

A Rosemount icing probe (RICE) provided an indication of the presence of LW and an estimate of the liquid water content (LWC) above its detection threshold of approximately 0.002 g m^{-3} (Heymsfield and Miloshevich 1989). Droplets and ice particles were collected on oil-coated slides exposed to the airstream (in association with N. Knight), although it was almost always impossible to distinguish droplets from ice using these observations alone, as the ice was generally small and spherical. Concentrations of ice particles larger than 37 μm (Sabreliner) and 25 μm (King Air) were measured with PMS two-dimensional imaging probes (2D-C and 2D-P).

Saturation ratio measurements are derived from the newly developed cryogenic frostpoint hygrometer

[1] In this paper, we will broaden the conventional meaning of "homogeneous" or "spontaneous" ice nucleation to be the process whereby droplet freezing is initiated when an ice embryo forms from water molecules within a *solution* droplet that has formed on a soluble cloud condensation nucleus (CCN).

[2] Throughout this paper, the term "droplet" will refer to liquid phase cloud particles of *all* sizes, including "unactivated haze particles," that may exist under subsaturated conditions.

FIG. 1. Photograph of lenticular wave clouds taken on 29 November 1990 looking north from Boulder, Colorado (photo by Bob Bumpas, NCAR). The downwind direction is toward the right.

(Spyers-Duran 1991; NCAR Tech. Note No. 347, available from NCAR) on the Sabreliner but must be inferred from the Lyman-alpha device (Buck 1976) on the King Air. The cryogenic hygrometer is a chilled-mirror device whose fast time response (2 s) results from the use of liquid nitrogen as a heat sink. The accuracy of the hygrometer under operational research conditions has not previously been established, and its performance characteristics are investigated within the present study. The voltage signal from the Lyman-alpha device is in theory linearly related to the vapor density (Spyers-Duran and Schanot 1987) and can therefore be calibrated for relative humidity measurement during selected time intervals where the vapor density is thought to be saturated with respect to either liquid or ice (based on the RICE and FSSP measurements), following the technique given by Heymsfield et al. (1991).

3. Aircraft measurements

Orographic wave clouds, especially lenticular (Fig. 1), provide conditions conducive to the study of cloud particle growth and ice nucleation. The low-turbulence, streamlined air flow in the sampled clouds, as verified by pilot reports, allows parcel trajectories and microphysical properties to be characterized. These clouds remained relatively unchanged, microphysically and dynamically, over a period of hours as aircraft penetrations stepped up and down in altitude through the cloud, always observing the same microphysical processes seen in the data presented in this section.

The NCAR Sabreliner flew five research missions in orographic wave clouds along the Front Range of the Rocky Mountains during November and December of 1989. The flights included 5 cloud penetrations between −25° and −30°C, 19 penetrations between −30° and −40°C, and 6 penetrations below −40°C. We also consider one research flight of the NCAR King Air on 8 December, consisting of 18 cloud penetrations between −30° and −41°C, in the same cloud sampled by the Sabreliner two hours earlier in this day. The aircraft flew reciprocal legs parallel to the wind direction between the leading (upwind) and trailing (downwind) edges of the cloud at constant altitude. Since constant-altitude sampling crosses streamlines, changes in individual parcel properties were not observed; the resulting geometrical effects and limitations on data interpretation are addressed in section 4.

In this section we present data from five cloud penetrations taken from three of the research flights selected as being representative of the cloud properties encountered in the temperature range −29° to −41°C. Three of these examples, the 8 December cases, sampled the same cloud at various temperatures between −31° and −41°C; thus, observations on this day should not reflect regional or temporal variations in aerosol characteristics.

The penetration data shown in Figs. 2–6 are numbered sequentially in order of decreasing temperature for all but Fig. 6, with an appended "S" (Sabreliner) or "K" (King Air) to indicate the aircraft involved. All data are plotted as a function of horizontal distance downwind from some initial point along the mean wind direction; the use of horizontal distance coordinates facilitates interpretation of the measurements in terms of approximate particle growth times given typical horizontal wind speeds of about 20 m s^{-1}. Aircraft altitude variation during a penetration was up to 100 m for the Sabreliner, so temperature curves adjusted to a constant altitude are shown for reference in these cases, as described in the Fig. 2 caption.

Penetration 1-S (Fig. 2), with minimum temperature $T_{min} \approx -29.2$°C, shows characteristics expected of droplet growth and evaporation in a wave but shows no evidence of significant ice production. The RICE and FSSP signals are above their respective detection

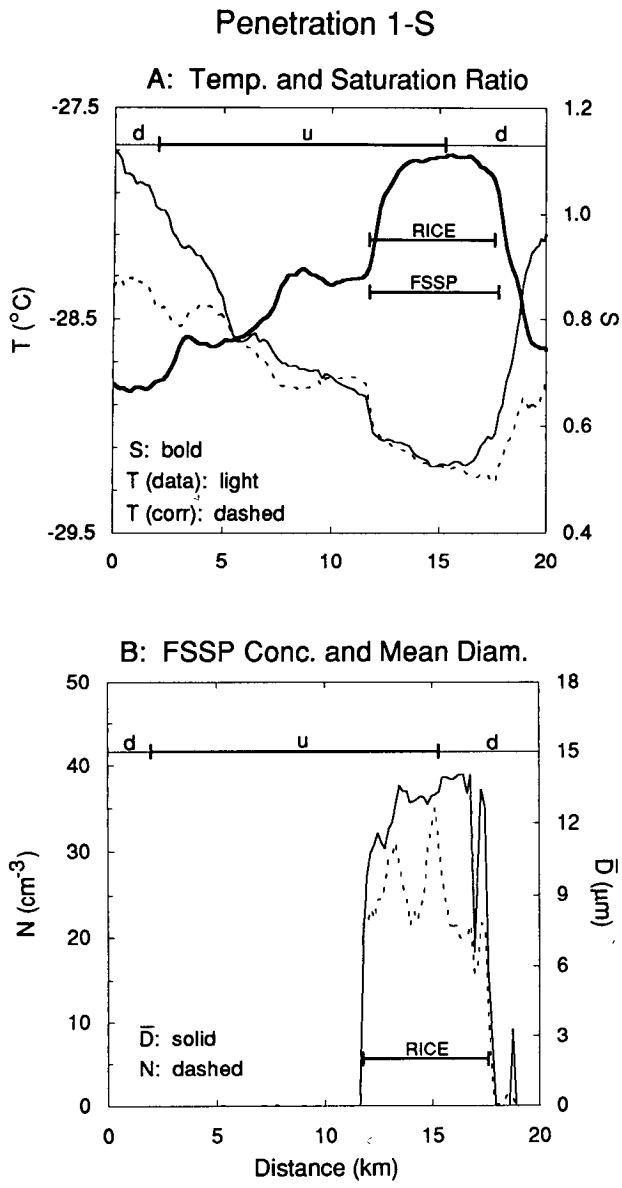

FIG. 2. Measurements from the Sabreliner taken on 9 November 1989 during the time period 1108:57–1110:59 MST. (a) Saturation ratio with respect to liquid (S) from the cryogenic hygrometer and temperature (T). A derived temperature curve that corrects for variation in aircraft altitude [labeled "T(corr)"] is shown for reference, where a reasonable mean between the ice saturated and dry adiabatic lapse rates of $-9°C\ km^{-1}$ was assumed. This correction was negligible for the King Air penetrations. Labeled horizontal bars indicate regions of detection of LW by the RICE, detection of cloud particles (droplets or ice) by the FSSP (in concentrations $\geq 1\ cm^{-3}$), and regions of updraft or downdraft (labeled "u" or "d," relative to $W = 0\ m\ s^{-1}$). (b) Total particle concentration (N) and mean diameter ($\bar{D}$) from the FSSP.

thresholds over approximately the same region, indicating that LW exists throughout the cloud width, and these signals coincide with the region of high saturation ratio[3] (panel a). Concentrations of particles detected by the 2D-C (not shown) were less than $0.3\ L^{-1}$, suggesting that few ice particles formed since the relative humidity in the downdraft is highly ice supersaturated, and any ice crystals present would grow to 25 μm in approximately 50 s or 1-km horizontal distance. Furthermore, the RICE, FSSP, and saturation ratio signals are centered on and are roughly symmetric about the wave crest (i.e., the minimum temperature or the beginning of the downdraft), as expected for droplet growth and evaporation under conditions of adiabatic ascent and descent.

Penetration 2-S (Fig. 3), with $T_{min} \approx -36.0°C$, shows a complement of instrument signals that indicate the presence of droplets in an updraft followed by an abrupt transition to ice. The RICE and FSSP first show signals that exceed their detection thresholds in the updraft when the saturation ratio with respect to liquid is approximately 1.0 (panel B, at distance coordinate $x = 15$ km), suggesting these cloud particles are droplets. The FSSP continues to detect cloud particles throughout the penetration, but the RICE ceases to detect LW at approximately the location where the saturation ratio drops below 1.0 (panel B, $x = 18$ km). Since the updraft speed is near its maximum of $2\ m\ s^{-1}$ (panel A, $x = 18$ km), it appears that droplets have frozen rather than evaporated. Simultaneously, the FSSP-detected mean particle diameter increases abruptly from 5 to 13 μm (panel C, $x = 18$ km), as would be expected if ice nucleated and rapidly grew in this initially highly ice-supersaturated environment. (Particle sizing by the FSSP may be inaccurate if the particles are ice crystals, but the abrupt shift clearly indicates a significant change in hydrometeor properties.) Following the apparent phase transition, significant concentrations of larger particles are detected by the 2D-C (panel D, $x > 18$ km) and the air is maintained at approximately ice saturation throughout the downdraft (panel B, $x > 18$ km). (The agreement of the cryogenic hygrometer measurements with the ice-saturation curve is an indication of the instrument's accuracy under these conditions of temperature and nearly constant saturation ratio.) Were the posttransition particles still liquid, the water content calculated from the FSSP size spectra would be 0.06 to 0.14 $g\ m^{-3}$, well above the RICE detection threshold of about 0.002 $g\ m^{-3}$.

[3] Several of the cases presented in this section imply hygrometer measurements of up to 10% supersaturation with respect to liquid, uncommonly high values in comparison with other cloud environments. These high values, supported by modeling calculations discussed in the Appendix, result from the dominance of the vapor supply in several meters per second updrafts compared to the much slower vapor depletion by growing droplets, with concentrations of order $100\ cm^{-3}$, at cold temperatures.

In penetration 3-S (Fig. 4), with $T_{min} \approx -37.6°C$, a narrow peak in saturation ratio exceeds 1.0 (panel B, $x = 10$ km), then immediately decreases to ice saturation; however, the RICE detects no LW and the FSSP shows no evidence of the abrupt change in mean diameter seen in the previous penetration (except as a change from zero to nonzero). The saturation ratio observations suggest that LW existed briefly, but the LWC at this temperature may have been below the detection threshold of the RICE, and droplet diameters may be smaller than the detection threshold of the FSSP. If the FSSP-detected particles were liquid, the LWC of about 0.01 g m^{-3} would have been detectable by the RICE. The high ice concentrations detected by the FSSP[4] are evidently capable of rapidly reducing the vapor density and maintaining the air at ice-saturation even in a 7 m s^{-1} updraft. The temperature ceases its steady decline at the same location as the rapid decline in saturation ratio and the onset of FSSP-detectable particles (panel A, $x = 10$ km), suggesting the release of latent heat may have affected the temperature. [Note the "undershooting" of the cryogenic hygrometer signal at this location, an instrument response that occurs when the detected saturation ratio is changing very rapidly.] Once formed, the ice alternately sublimates in the downdrafts and grows in the updrafts (panels C and D, solid curves), until it eventually disappears and the air becomes subsaturated with respect to ice (panel B, $x = 40$ km). Near the end of the penetration, the saturation ratio again increases above ice saturation but without producing detectable particles.

Penetration 4-K (Fig. 5), with $T_{min} \approx -40.7°C$, is similar to penetration 3-S in that FSSP particles are first detected in the midst of an updraft (4.5 m s^{-1}) at the location where the saturation ratio abruptly decreases and the temperature ceases its rapid decline (panel A, $x = 7$ km). The Lyman-alpha data suggest that the peak saturation ratio is below 1.0; however, the linearity of the instrument's response is questionable when vapor densities are below 0.3 g m^{-3} (A. Schanot, private communication), as is the case here.

Penetration 5-K (Fig. 6), with $T_{min} \approx -31.7°C$, shows the complement of simultaneous, abrupt instrument signals seen in Fig. 3, which characterize the transition from a liquid-dominated to an ice-dominated environment (panels A and B at $x = 37$ km). Unlike Fig. 3, however, the *apparent* phase transition in Fig. 6 occurs in the downdraft, an initially unexpected observation since colder temperatures were encountered and larger droplets remained unfrozen at the location of the wave crest ($x = 30$ km). This ice presumably formed at some lower temperature above the aircraft sampling level, then descended in the downdraft, as will be demonstrated in the following section.

4. Discussion and implications of the aircraft measurements

In this section we will examine whether the measurements presented in section 3 are consistent with the homogeneous ice nucleation process. The conditions for existence of supercooled liquid water, and the possible relevance of homogeneous ice nucleation to cirrus and altocumulus clouds, will also be discussed.

a. Are the measurements qualitatively consistent with homogeneous ice nucleation?

Evidence is provided by the large droplet diameters and lack of ice seen in Fig. 2 at −29.2°C and in Fig. 6 at −31.6°C that no *heterogeneous* ice nucleation mechanism seems to be important down to these temperatures in the wave clouds. Furthermore, these cases indicate that no significant freezing mechanism is operative here that occurs in the downdraft portion of the wave as a result of droplet evaporation.

The observations at temperatures above −36°C (Figs. 3 and 6) demonstrate instrument signatures expected to be characteristic of homogeneous ice nucleation. Given the strong temperature dependence of homogeneous ice nucleation rates, the relatively rapid observed cooling rates (strong updraft speeds) should result in an abrupt transition from droplets to ice. Therefore, the following simultaneous complement of instrument responses should reflect the changes in cloud properties resulting from homogeneous ice nucleation: disappearance of LW detected by the RICE; decrease in relative humidity derived from the cryogenic hygrometer or the Lyman-alpha from a peak near water saturation to near ice saturation; changes in mean particle diameter and particle concentration as measured by the FSSP (which may not be quantitatively accurate but which indicate a change in hydrometeor properties); and successive detection of signals from the FSSP then 2D-C then 2D-P probes, where each instrument has a successively larger size detection threshold.

Below −36°C the rapid decline in relative humidity from liquid-supersaturated to ice-saturated conditions, characteristic of droplet freezing at temperatures above −36°C, is again detected (Figs. 4 and 5). These penetrations also show an abrupt and simultaneous shift

[4] The ice particle concentrations measured by the FSSP in these wave clouds ($\sim 10^4$–10^5 L^{-1}) are unusually high in comparison to most other cloud environments. Spurious particle counts are known to be produced by ice crystals that exceed the upper size detection limit of the FSSP (Gardiner and Hallett 1985; Heymsfield and Miloshevich 1989). Modeling calculations discussed in the Appendix support the assertion that these high values are not the result of spurious FSSP counts but arise from the very rapid freezing rates attainable in a strong updraft compared to droplet evaporation rates. The observed ice size spectra are strongly peaked, unlike the flat size distributions characteristic of spurious counts. Furthermore, in situ slide collections show the ice particles to be small and spherical.

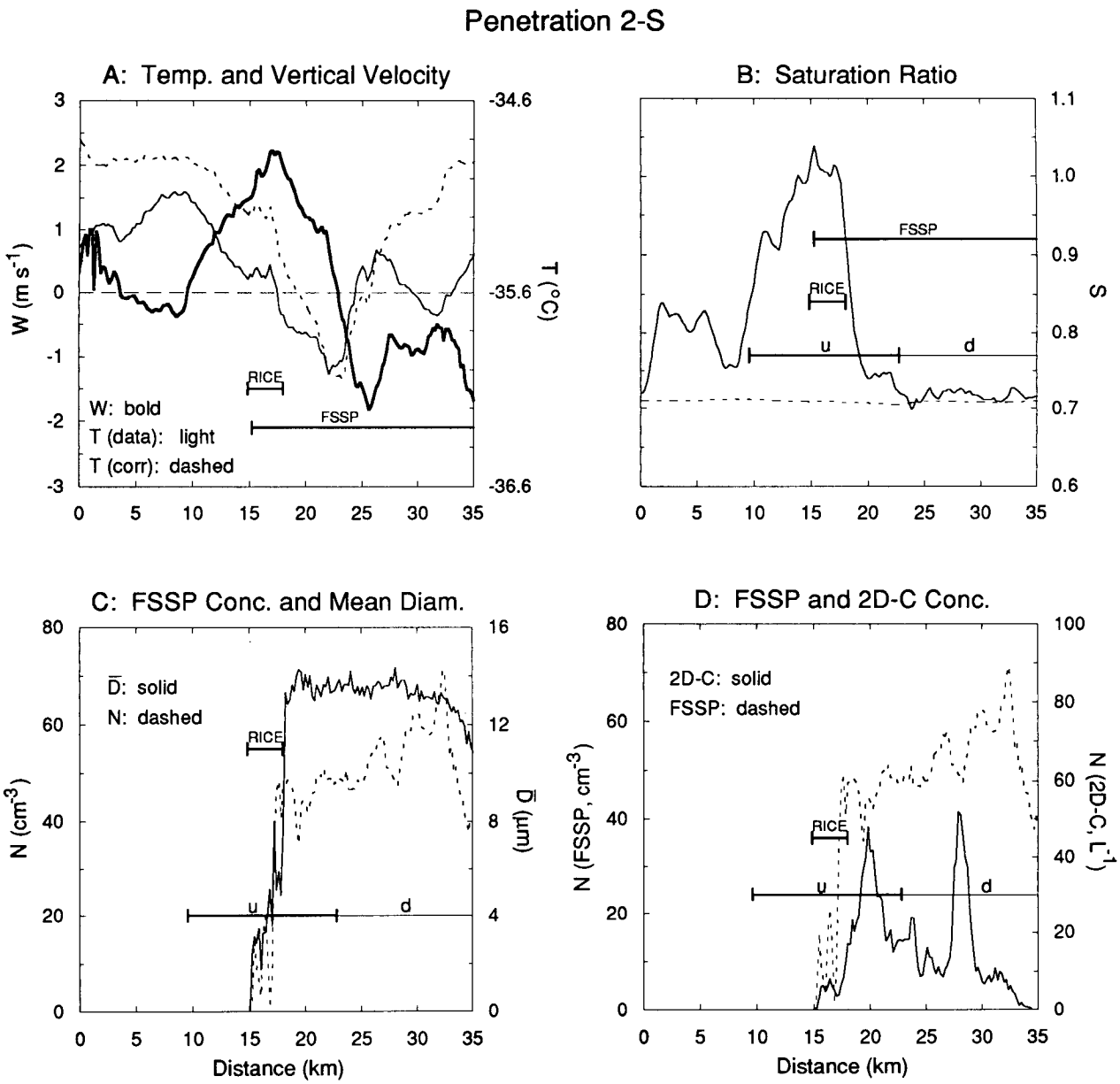

FIG. 3. Measurements from the Sabreliner taken on 9 November 1989 during the time period 1200:40–1203:38 MST. Labeled horizontal bars are defined as in Fig. 2. (a) Vertical velocity (W) and temperature (T); (b) saturation ratio with respect to liquid (S) from the cryogenic hygrometer. Dashed reference curve is the saturation ratio that corresponds to ice-saturated conditions. (c) Total particle concentration (N) and mean diameter ($\bar{D}$) from the FSSP; (d) total particle concentrations from the FSSP and the 2D-C.

in the rate of change of temperature measured along the flight path, which may result from the release of latent heat upon ice nucleation (where a simple calculation shows that the conversion of liquid and excess vapor to ice should warm the air by about 0.3°C). The simultaneous ice nucleation signal from the RICE seen at temperatures above −36°C is absent at these temperatures, presumably the result of signals that fell below the detection threshold of this instrument (as will be discussed shortly). If droplets exist yet are undetectably small just prior to ice nucleation, the FSSP should then detect ice almost immediately upon freezing since ice growth rates are approximately 0.5 μm s^{-1} for the highly ice-supersaturated conditions that exist when ice nucleation begins. We conclude that the complement of instrument signals seen in Figs. 4 and 5, especially the abrupt decrease in relative humidity followed immediately by the first FSSP-detectable par-

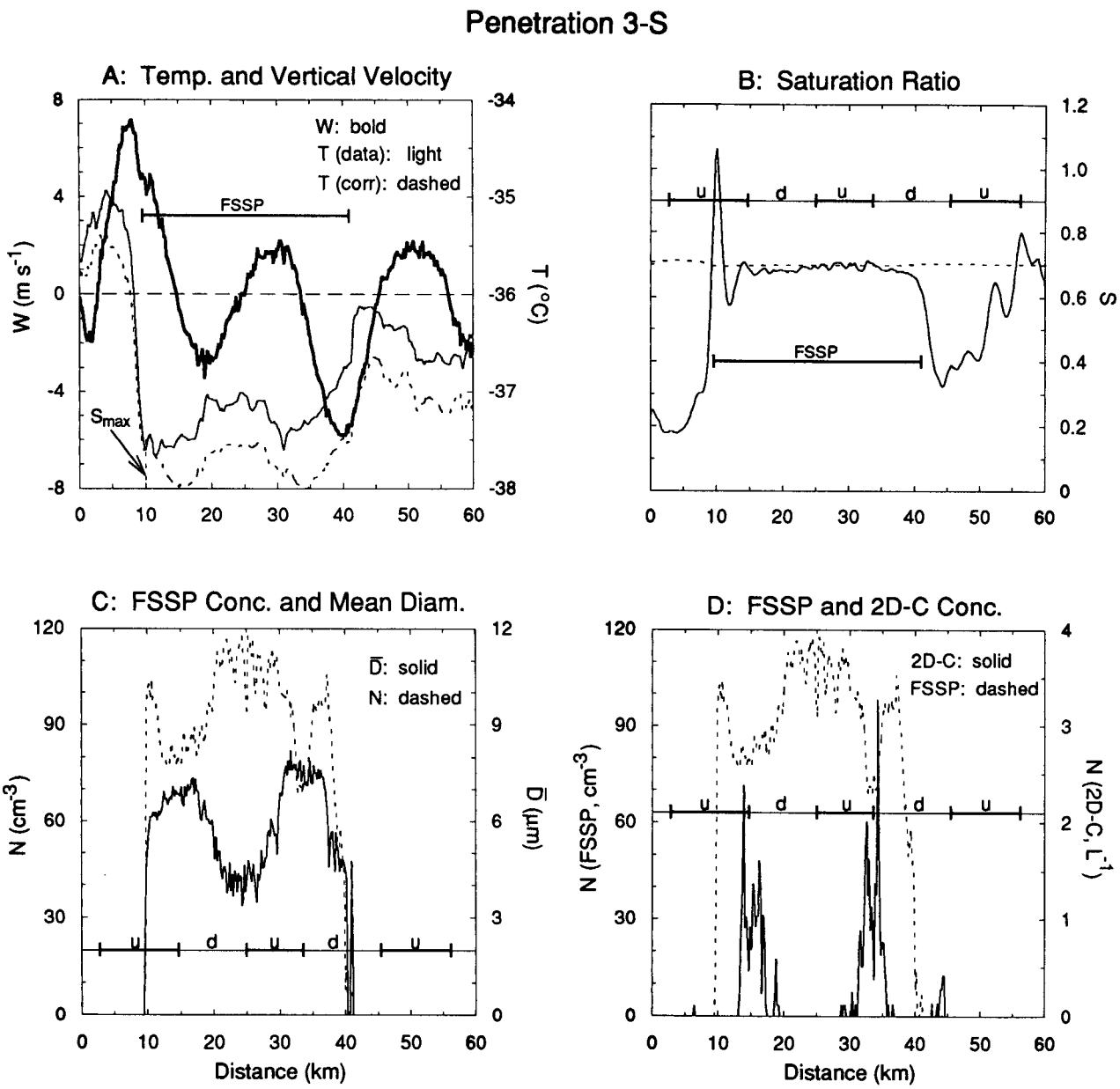

FIG. 4. Measurements from the Sabreliner taken on 8 December 1989 during the time period 1315:00–1321:02 MST. All curves and symbols are the same as in Fig. 3. Also shown in (a) is the location of the peak saturation ratio taken from (b) (labeled "S_{max}").

ticles, suggests the freezing of very small (i.e., undetectable) droplets at temperatures below −36°C.

To investigate more objectively the instrument signals expected to be characteristic of homogeneous ice nucleation, we draw upon modeling of this process in a wave cloud so as to make qualitative comparisons with the observations. The 1D numerical model employed in this study performs a time-dependent integration of coupled ordinary differential equations describing state parameters, growth rates of solution droplets in 20 CCN mass categories, homogeneous freezing rates for each category (discussed in detail in the next subsection), and ice crystal growth rates. The 2D wind field along a parcel trajectory is specified. Droplets are assumed to form on ammonium sulfate CCN, and ice crystals to be spheres, which grow with a density of 0.7 g cm^{-3}. Solute and curvature effects are included in the droplet growth and homogeneous freezing rates through their effect on the equilibrium vapor pressure over the droplets (Byers 1965). The

model is initialized by specifying values for the thermodynamic variables, the vertical velocity profile, and the constants C and k that define the power-law form of the CCN mass spectrum. The numerical integration scheme employs a variable time step technique that preserves a specified level of accuracy in all simulation variables (with time steps as small as 0.001 to 0.01 s when conditions are changing rapidly, as during ice nucleation). A more complete description of the model is given in Heymsfield and Sabin (1989), and a detailed analysis of its application to liquid phase altocumulus clouds is given in Heymsfield et al. (1991).

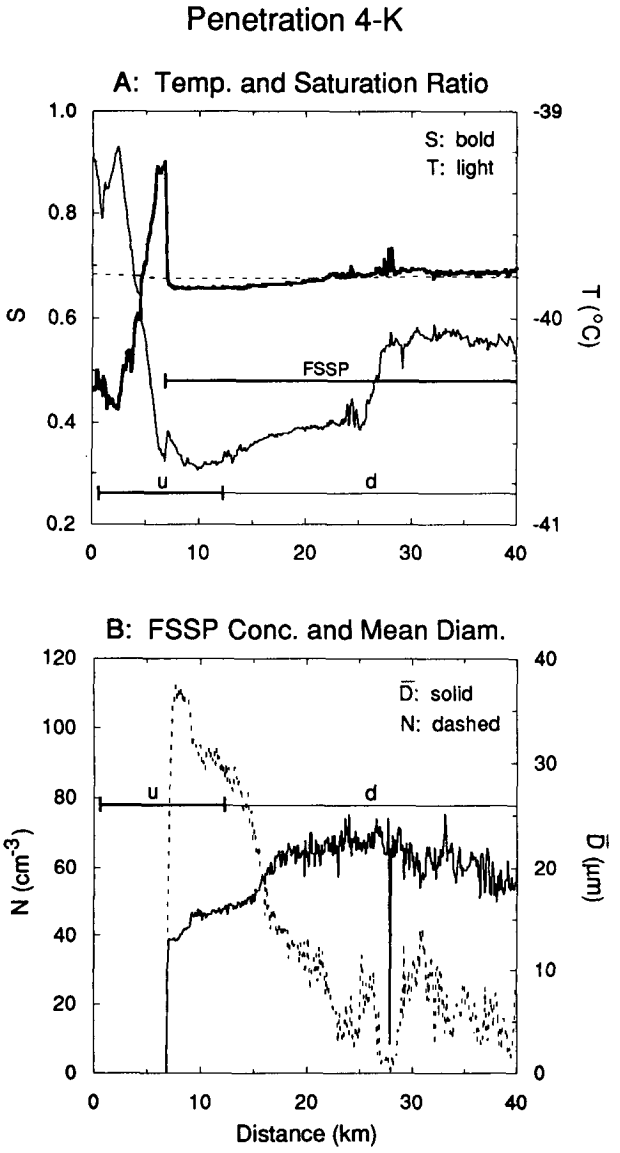

FIG. 5. Measurements from the King Air taken on 8 December 1989 during the time period 1057:00–1107:00 MST. All curves and symbols are the same as in Fig. 2 except that the saturation ratio is derived from the Lyman-alpha measurements. Calibration of the Lyman-alpha voltage for vapor density uses the linear fit $\rho_v = A + BV$, where $A = 3.229$ g m^{-3} and $B = 3.421$ g m^{-3} V^{-1}. Data courtesy of W. (Al) Cooper, NCAR.

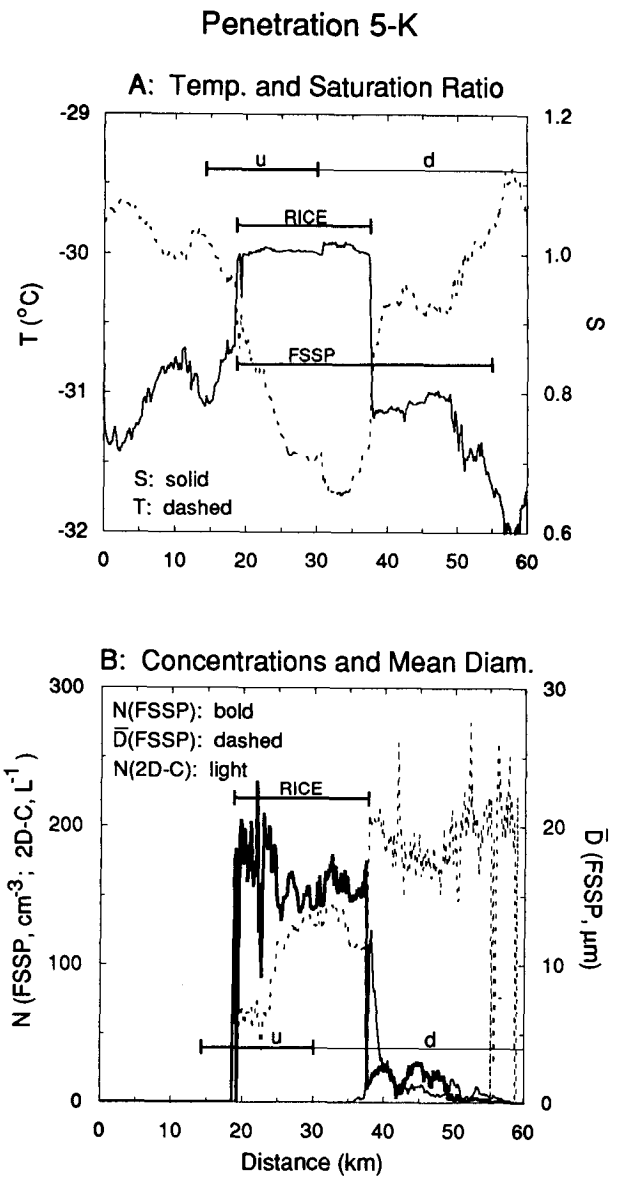

FIG. 6. Measurements from the King Air taken on 8 December 1989 during the time period 0918:40–0925:58 MST. All curves and symbols are the same as in Fig. 2 except that the saturation ratio is derived from the Lyman-alpha measurements. Calibration of the Lyman-alpha voltage for vapor density uses the linear fit $\rho_v = A + BV$, where $A = 3.229$ g m^{-3} and $B = 0.716$ g m^{-3} V^{-1}. Data courtesy of W. (Al) Cooper, NCAR.

Model results of the phase of condensed water in a hypothetical wave cloud are shown schematically in Fig. 7 for a vertical cross section parallel to the wind direction along several streamlines. Each model run (i.e., each streamline) was initialized at the start of

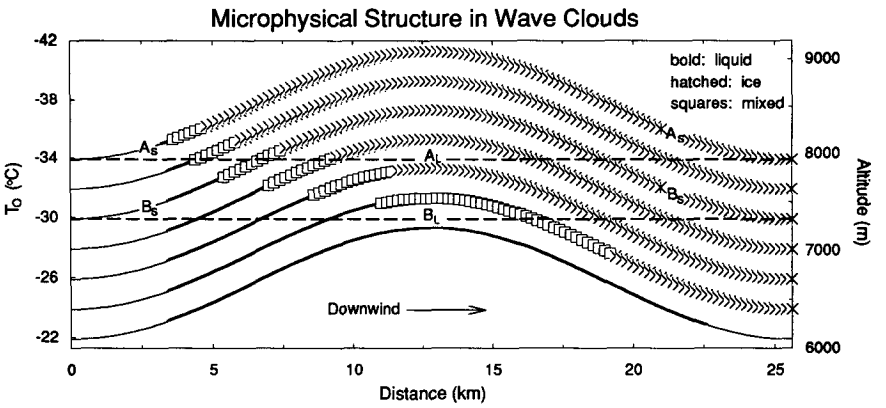

FIG. 7. Set of model-generated streamlines representing a vertical cross section along the wind direction through a hypothetical wave cloud. Symbols represent regions of liquid (bold), ice (cross hatched), and mixed-phase (squares). The left ordinate is initial upstream temperature in the unforced environment, assuming an ambient lapse rate of $-6.5°C\ km^{-1}$. Other model assumptions are given in the text.

uplift (distance = 0 km) at relative humidity 85%,[5] assuming homogeneous freezing to be the only ice nucleation mechanism. This cloud model is not intended to describe the wave clouds encountered in this study, and the unrealistic, constant upstream humidity profile is employed to simplify understanding of the effects of temperature and vertical velocity on the cloud microphysics. Additional model parameters, loosely based on the aircraft measurements presented earlier, are a stably stratified upwind environmental lapse rate of $-6.5°C\ km^{-1}$, a sinusoidal vertical velocity profile of peak magnitude 280 cm s^{-1} and wavelength 25.6 km with no wind shear, and a horizontal windspeed of 20 m s^{-1} everywhere. Note that the left ordinate (T_0) represents *initial* parcel temperatures at 85% relative humidity, and since subsequent parcel temperature changes in the vertical are adiabatic, *temperature at a given altitude across the cloud is not constant.*

In Fig. 7, the model suggests that LW should exist at the leading edge and lower levels of the cloud; however, the start of condensation at a given level in the cloud depends on the assumed upstream humidity profile. The increase in ice nucleation rate with decreasing temperature is apparent in the decreasing widths of the liquid-phase and mixed-phase regions with altitude.

[5] All model runs considered in this paper are initialized at 85% relative humidity rather than at "cloudbase" (i.e., approximately 100% relative humidity) for several reasons: 1) 85% relative humidity is near the deliquescence point of ammonium sulfate CCN, 2) the rate at which droplets freeze homogeneously depends on the droplet diameter, which would be significantly overestimated if "equilibrium diameters" at cloudbase were assumed initially, and 3) homogeneous freezing at cold temperatures (e.g., $< -40°C$) can occur in unactivated droplets at relative humidities below 100%.

The microphysical and thermodynamic properties of the wave cloud modeled in Fig. 7, along the two streamline paths A_S and B_S and along the two level paths A_L and B_L, are developed and presented in the Appendix. These model results agree qualitatively with the observations and with the previously stated complement of instrument responses expected from homogeneous ice nucleation: an abrupt disappearance of liquid water, a decrease in relative humidity from near water saturation to ice saturation, an increase in mean particle diameter and a change in particle concentration, and an indication of latent heat release.

b. Homogeneous ice nucleation rates

We must employ *indirect* means to assess ice nucleation rates from the data since we believe that *direct* calculation of the rates from measured LWC and subsequent cloud glaciation times are inappropriate at the present time for at least the following four reasons.

- Detection thresholds of the RICE and FSSP instruments prevent detection of droplets and measurement of LWC at temperatures below about $-36°C$ (see discussion in the Appendix and Fig. A2), hence direct calculation of ice nucleation rates is not possible at temperatures below about $-35°C$.
- Even at temperatures above $-35°C$, calculation of ice nucleation rates will be in error since some unknown fraction of the droplets and LWC evaporates during the ice nucleation process when growing ice particles lower the relative humidity. The magnitude of this effect, manifested in part by the observed shift in FSSP-detected particle concentrations (e.g., Fig. 6b, $x = 37$ km), varies greatly as a function of temperature and updraft speed, as will be shown numerically later in this subsection.

• An aircraft sampling along a level flight path in a wave cloud traverses streamlines; thus, microphysical properties along a single parcel trajectory are not observed. As shown in Fig. 7 (along paths A_L and B_L), air parcels are sampled that originated upwind at different altitudes with different thermodynamic properties and that underwent different degrees of uplift and hence have different particle growth histories. Direct calculation of observed ice nucleation rates is yet more uncertain when aircraft flight paths involve altitude change or are not along the wind direction (e.g., Sassen and Dodd 1988).

• Modeling studies show that measurable properties that depend upon the homogeneous ice nucleation rates are relatively insensitive to those rates. An increase or decrease in the ice nucleation rate at a given temperature by a factor of 10^2 will change the ice concentration produced from a given droplet concentration by at most a factor of 2 and will change the temperature at which the cloud becomes glaciated by less than 1°C. Thus, observational uncertainties correspond to uncertainties in ice nucleation rates of about two orders of magnitude.

Ice nucleation rates employed by the model are taken from the statistical molecular approach of Eadie (1971). This theoretical model predicts the thermodynamic properties of liquid water satisfactorily, and the rates compare favorably (see Heymsfield and Sabin 1989, Fig. 2) with recent laboratory measurements by DeMott and Rogers (1990) and with the aircraft and lidar measurements reported by Sassen and Dodd (1988). The theory applies over a temperature range from −30° to −50°C, whereas the above experimental data have been derived over a temperature range of only −35° to −38°C and any extrapolation outside this temperature range cannot be justified. The ice-nucleation rates for pure, bulk water ($J_{H,0}$; number of ice embryos formed per cubic centimeter of water per second) are given by a polynomial curve fit to the values Eadie derived:

$$\log J_{H,0} = -\sum_{i=0}^{4} A_i T^i, \qquad (1)$$

where T is measured in degrees Celsius and $A_0 = 606.3952$, $A_1 = 52.6611$, $A_2 = 1.7439$, $A_3 = 0.0265$, and $A_4 = 1.536 \times 10^{-4}$. The homogeneous ice nucleation rates for *solution* droplets (J_H) include depression of the freezing point due to solute and curvature effects on the equilibrium vapor pressure over the droplets (Byers 1965); these effects are only significant when droplets are small (<1–2 μm), and therefore $J_H \approx J_{H,0}$ for all cases where droplets are observable by the RICE or FSSP.

The homogeneous ice nucleation rates (J_H) and the associated droplet freezing rates ($J_H VN$, where N is the concentration of droplets having volume V; number of *droplets* frozen per cubic centimeter of *air* per second) are both shown in Fig. 8 for two different assumed CCN masses. The increase in *instantaneous* ice

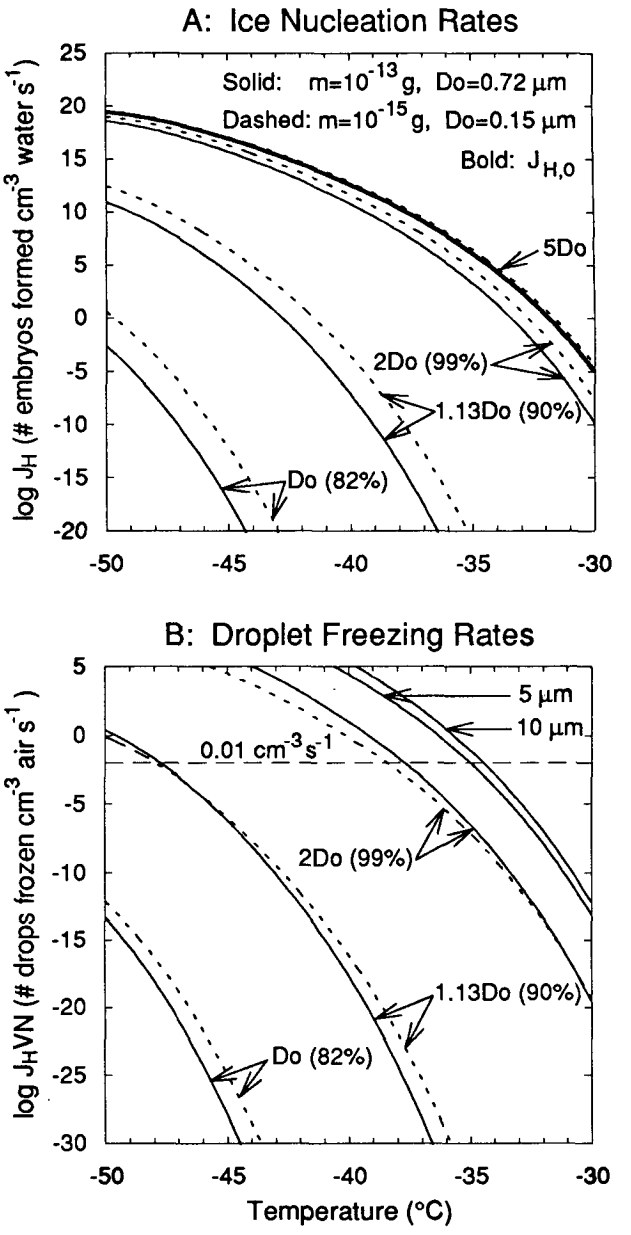

FIG. 8. Ice nucleation rates (a) and droplet freezing rates (b) employed in the model. Shown in (a) are the nucleation rates for pure, bulk water ($J_{H,0}$) given by Eq. (1) and the rates for solution droplets of several sizes containing one of two different ammonium sulfate CCN masses. Droplet diameters are given in terms of D_0, the equilibrium droplet size at the point of deliquescence (82% relative humidity). Percentages indicate the relative humidity at which droplets of the given size are in equilibrium. Shown in (b) are the corresponding droplet freezing rates, equal to J_H multiplied by an individual droplet's volume (V) and total concentration of droplets of that size (N, assumed here to be 100 cm^{-3}).

nucleation rates and droplet freezing rates with decreasing temperature and increasing droplet size is apparent. Figure 8 demonstrates the following properties of the homogeneous freezing mechanism.

- Vapor pressure depression resulting from dissolved solute effectively prevents freezing of solution droplets at the point of deliquescence (82% relative humidity when droplets consist of a saturated solution of ammonium sulfate). As a result, very small liquid phase "haze particles" are expected to exist even at temperatures below −50°C (panel B). Some amount of droplet growth beyond deliquescence is necessary before droplet freezing rates become significant.
- A significant homogeneous droplet-freezing rate ($J_H VN$) can occur over a very wide range of temperature for different droplet sizes, as seen along the reference line in panel B, which indicates a droplet freezing rate of 0.01 cm^{-3} s^{-1}. This wide temperature range results primarily from the different temperatures at which droplet deliquescence may occur, and the consequent depression of the homogeneous ice nucleation rate by high solute concentrations in small droplets. Larger droplets will freeze quickly in a narrow temperature range of a few degrees around −35°C; thus, an assumption of a specific homogeneous freezing temperature is nearly appropriate for these "warm" cases involving nearly pure water droplets.
- Droplets in an updraft simultaneously experience growth and transport to regions of lower temperature, thus time evolution in Fig. 8 would proceed both vertically (corresponding to droplet growth and a decrease in solute and curvature effects) and to the left. Note that droplet freezing rates cannot be traced in time since Fig. 8b assumes a specific droplet concentration (100 cm^{-3}), and freezing will decrease droplet concentrations below this initial value, as well as lead to evaporation of remaining droplets as ice crystals grow and deplete the vapor supply.

We can *indirectly* compare the observations of ice nucleation and the modeled ice nucleation rates by evaluating the effect of J_H on the following measurable parameters: 1) the temperature at which droplets of a given size freeze, 2) the temperature at which droplets of the minimum size detectable by the RICE freeze, and 3) the magnitude of the change in FSSP-detectable particle concentrations upon ice nucleation. Since the rate at which droplets of some particular volume and concentration freeze is given by $J_H VN$, there is a specific temperature at which droplets of a particular diameter will freeze homogeneously at a rate great enough to produce cloud glaciation within the observed few seconds of *aircraft* sampling time ($J_H VN \approx 10^{-2}$ to 10^{0} cm^{-3} s^{-1}).

To discern from the measurements the temperature at which ice nucleates, consider first an aircraft that flies along a level path in a wave cloud, such as path A_L or B_L in Fig. 7. When the freezing event is detected in descending air (Fig. 6), ice nucleation must have occurred upwind and at some higher altitude and colder temperature (as in Fig. 7, B_L); thus, the phase transition detected at a temperature of −31.7°C in Fig. 6 *does not* represent the temperature at which ice nucleation occurred. In contrast, when the freezing event is detected in ascending air (Figs. 3–5), successive stages in the ice nucleation process have been observed in nearby parcels (as in Fig. 7, A_L). Since ice nucleation is observed to occur abruptly over a short horizontal distance and narrow temperature range, reflecting small differences in the amount of uplift experienced by nearby parcels, we can infer that ice nucleation occurred within the narrow temperature range of the observed phase transition. Therefore, the temperature of about −35.7°C at the detected freezing event in Fig. 3 is approximately the temperature at which ice nucleation occurred.

The observations from Fig. 3 show that 5-μm droplets freeze at a temperature of about −35.7°C, in agreement with the model-predicted droplet diameter that freezes at this temperature, taken from Fig. 8b when $J_H VN \approx 10^{-1}$ cm^{-3} s^{-1}. Ice nucleation in Fig. 4, based on the relative humidity signal, occurs at about −37.6°C, in agreement with the expected ice nucleation temperature from Fig. 8b if droplet diameters are about 2 μm. Droplets are not observed in Fig. 4; however, droplets smaller than about 3 μm are not detectable with the RICE or FSSP (as discussed in the Appendix). Finally, the large droplets and lack of ice nucleation seen in Fig. 2 are consistent with the extremely low homogeneous freezing rate expected at −29.2°C.

A related means of assessing the observed ice nucleation rates considers the temperature at which droplets freeze just prior to attaining the sizes required for detection by the RICE (shown in the Appendix to be approximately 3 μm if droplet concentrations are 100 cm^{-3}). Figure 9 compares the RICE output voltage signal for all aircraft flights to the calculated RICE signals for a series of model runs initialized at successively lower temperatures (where the RICE signal is linearly proportional to the LWC). The aircraft measurements shown in Fig. 9 indicate that no significant concentration of droplets larger than 3 μm is sensed by the RICE below about −36°C. The modeling calculations in Fig. 9 further show that droplets will freeze homogeneously before growing to the assumed 3-μm RICE detection threshold at a temperature of about −36°C. Also, Fig. 8b shows that $J_H VN \approx 10^{-1}$ cm^{-3} s^{-1} for 3-μm droplets at −36°C; thus, the model is in general agreement with the observations as to the temperature at which ice nucleation rates become rapid for 3-μm droplets. Better agreement in the temperature corresponding to the rapid decline in detectable LWC seen in Fig. 8 would result if our modeled ice nucleation rates were

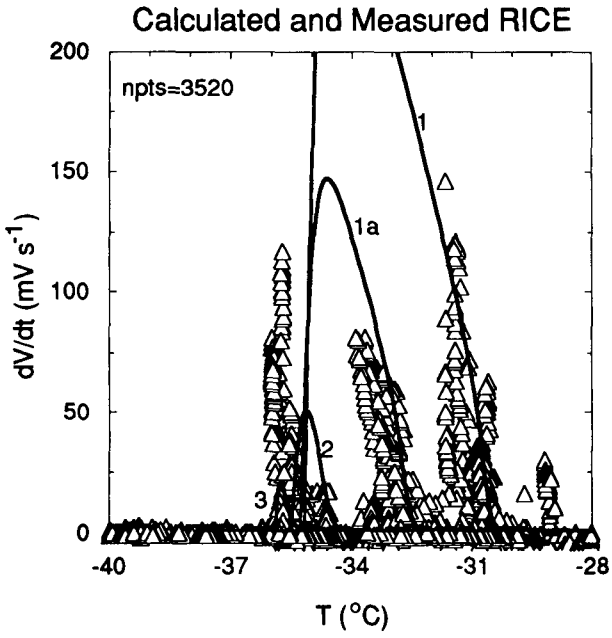

FIG. 9. Time derivative of the RICE voltage signal whenever FSSP concentrations exceed 1 cm^{-3} (triangles), excluding periods during and for 40 seconds following instrument deicing events when the signal is unstable. Curves are model calculations of RICE signals assuming an aircraft true airspeed of 150 m s^{-1} based on the calibration for LWC given by Heymsfield and Miloshevich (1989). Model runs assume a constant vertical velocity of 100 cm s^{-1} and are initialized at 85% relative humidity with different initial temperatures of −28°C (labeled 1), −30°C (1a), −32°C (2), and −33°C (3). The power-law form of the assumed CCN mass spectrum is given by constants C and k of 62 and 0.5, respectively, which produces a total CCN concentration of about 100 cm^{-3}.

shifted to colder temperatures by about 1°C (corresponding to an increase in the ice nucleation rates by 1–2 orders of magnitude).

An additional means of investigating ice nucleation rates is to consider their effect on the magnitude of the abrupt change in FSSP-detectable particle concentrations before and immediately after freezing occurs, assuming that ice concentrations measured by the FSSP (but not necessarily the diameters) are reasonably accurate when the particles are small, spherical, recently frozen droplets. Figure 10a shows model calculations for the final ice concentration that results from a deliquesced CCN concentration of about 100 cm^{-3} as a function of the vertical velocity (W) and the temperature at which the CCN deliquesced (T_0). (For reference, the increase from 85% to 100% relative humidity at $T_0 = -35$°C requires 1.7°C of cooling.) Figure 10b is based on the same model runs, but the ordinate has been divided by the peak concentration of *detectable* droplets (≥3 μm); thus, this ratio is useful for comparison to the observations in that it considers the magnitude of change in FSSP-detectable particle concentrations when the cloud glaciates, including cases where ice nucleation occurs prior to some or all of the droplets attaining detectable sizes. The drastic increase in ice concentrations as W increases (Fig. 10a), indicative of ice nucleation that occurs on a time scale increasingly faster than droplet evaporation, demonstrates a measurable effect of the strong temperature dependence of J_H.

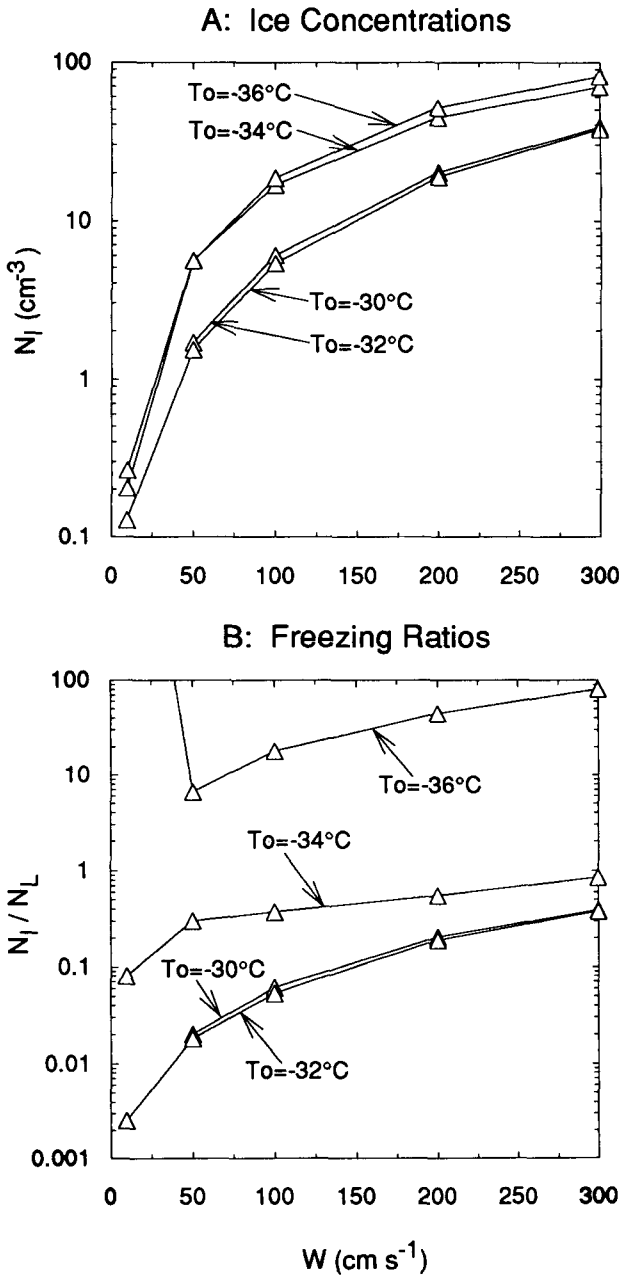

FIG. 10. Model results of ice concentrations (a) and the ratio of ice to droplet concentrations (b) as a function of uplift velocity (W) and initial temperature (T_0) at 85% initial relative humidity assuming a 3-μm minimum detectable droplet size, and the same CCN size spectrum used in the Fig. 9 model runs.

Qualitative comparisons can be made between the observations and the model calculations shown in Fig. 10. Quantitative comparisons require, at the minimum, reconstruction from the observations of vertical profiles of temperature and relative humidity along each parcel's path in order to determine T_0, as well as modeling of realistic (nonconstant) vertical velocity profiles and CCN distributions, which is beyond the intended scope of this study. The observed ratio of ice concentration to *detectable* droplet concentration increases with decreasing temperature in Figs. 3–5, as expected from Fig. 10b. The tendency toward a large ratio when $T_0 \leqslant -36°C$ results from the freezing of droplets while still smaller than the detection threshold of the FSSP, as we suggest is the case in Figs. 4–5 (and for a *portion* of the droplets in Fig. 3).

We conclude that the ice nucleation rates from the measurements are consistent with the modeled homogeneous ice nucleation rates (within a factor of 10^2) in the temperature range −35°C to −38°C because 1) the temperatures at which droplets of the measured sizes freeze are consistent with the modeled ice nucleation temperatures for those droplet sizes, 2) disappearance of RICE signals below about −36°C is within 1°C of the calculated temperature at which droplets freeze before reaching the 3-μm detection threshold of this instrument, and 3) the observed temperature dependence of the change in FSSP-detectable particle concentrations when droplets freeze is consistent with the trend given by the model. Given the rough agreement between Eadie's theory and the observations in the temperature range stated above, it is perhaps reasonable to consider his results to be useful throughout the −30°C to −50°C temperature range he considered.

c. *Minimum temperature for supercooled LW?*

Detection of LW by the RICE and FSSP in this study tends to zero at about −36°C, in agreement with model results presented in Figs. 9 and A2 and with previous research cited in the Introduction. The cryogenic hygrometer measurements, supported by numerical modeling, suggest this is not a fundamental low-temperature physical limit for the existence of water in the liquid phase. The model suggests that the maximum droplet sizes that can exist in the atmosphere decrease smoothly with decreasing temperature (although the rate of decrease is quite rapid around −36°C), as droplets freeze at smaller and smaller sizes, eventually below the detection thresholds of the RICE and FSSP. The saturation ratio, FSSP, and temperature measurements in Fig. 5 are strongly suggestive of the presence of LW at −40.7°C. The existence of LW at such cold temperatures theoretically results from depression of ice nucleation rates and the resulting inhibition of freezing of very small, unactivated droplets due to their high concentration of solute (see Fig. 8).

d. *Applicability of results to cirrus and altocumulus clouds*

The results presented thus far suggest that droplets freeze homogeneously when 1) the relative humidity increases to well above ice saturation, 2) the air temperature cools below about −35°C, and 3) parcels cool at a rate of at least 0.01°C s^{-1}, corresponding to a vertical velocity of about 1 m s^{-1}. Favorable conditions for all of these criteria could apply to isolated convective cirrus (uncinus and jetstream bands) and sometimes to embedded cirrus (Heymsfield 1977, Fig. 3b), as well as to cold altocumulus and deep convective clouds.

The model results presented in Fig. 10a suggest that relatively low concentrations of ice crystals (of order 10^{-1} to 10^0 cm^{-3}) should result under the low vertical velocity conditions (<10 to 50 cm s^{-1}) considered typical of cirrus formation, provided homogeneous ice nucleation is not preceded by other ice nucleating mechanisms so that condition 1) is not satisfied. These low modeled ice concentrations correspond roughly to measurements in cirrus when data have been collected down to 10-μm sizes. In such cases the dominant contribution to the total ice concentration is from particles smaller than 25 μm (Heymsfield and Platt 1984).

Other ice nucleation mechanisms, where aerosols can serve as "*deposition nuclei*" or as "*immersion nuclei,*" appear not to be a significant source of ice crystals at altocumulus and cirrus altitudes (Fig. 2; Fig. 4b at $x = 55$ km; Heymsfield et al. 1991; Sassen and Dodd 1988; Hobbs and Rangno 1985) compared with at lower altitudes, at least not at the parcel cooling rates encountered in this study. In situations where parcels are undergoing relatively slow cooling, however, homogeneous nucleation will be slower to operate and might not dominate the ice-formation process.

We propose the possibility that homogeneous nucleation may dominate ice production during the initial stages of cirrus *formation,* thus giving rise to the *first* ice particles. Homogeneous nucleation cannot continue to produce ice, except possibly at cloud top in ascending air, since the larger ice crystals expected from theory (>100 μm) would fall through the updraft, eventually reducing the vapor density at lower levels such that condition 1) is no longer satisfied. Crystal–crystal collisions and breakup offers one possible mechanism whereby the smaller ice crystals observed in cirrus can be continuously replenished.

e. *Summary of conditions for the occurrence of homogeneous ice nucleation*

Homogeneous ice nucleation places lower limits on the temperature at which LW can exist. Droplets in cold clouds *will* freeze homogeneously if heterogeneous nucleation mechanisms do not act first and at a temperature determined primarily by W, T_0, and probably by CCN characteristics. The vertical bars in Fig. 11

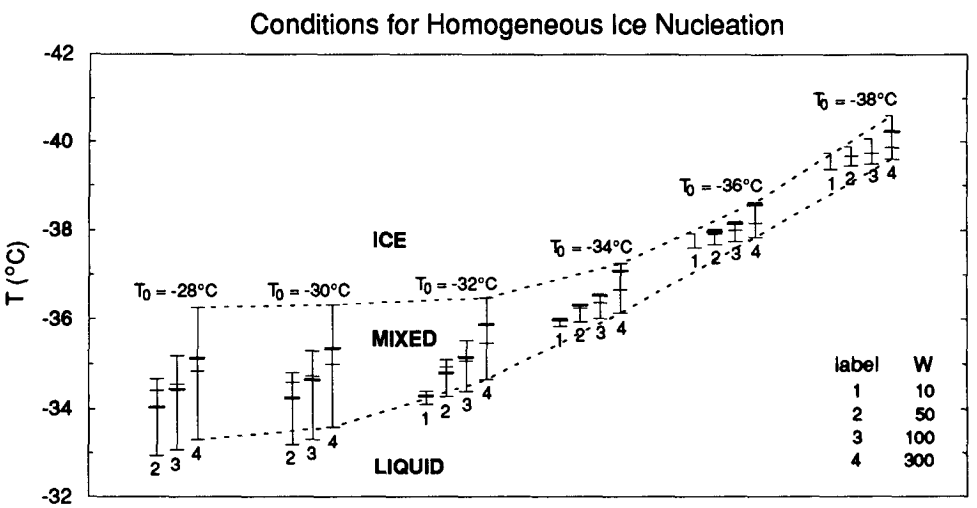

FIG. 11. Model results describing the temperature range over which the homogeneous ice nucleation process occurs, for a range of initial temperatures (T_0) and uplift velocities (W, cm s^{-1}), employing the same model parameters as in Fig. 9. The $W = 10$ cm s^{-1} runs when $T_0 \leq -30$°C are not included because they require excessive computer time and programming modifications. Symbols are further described in the text.

represent the temperature range over which the model suggests that appreciable homogeneous ice nucleation will occur for several conditions of W and T_0. The "beginning" of the freezing event (lower horizontal bars) is taken to be the temperature where ice concentrations first exceed 1L^{-1}, and the "end" of the freezing event (upper bars) is taken to be the temperature at which all droplets have either frozen or evaporated below measurable sizes (defined here to be 3 μm). These two temperatures, for a given W, define an "envelope" that describes temperature limits for the existence of liquid, ice, and mixed-phase conditions (e.g., the dashed lines that represent the $W = 300$ cm s^{-1} envelope). The two sets of intermediate horizontal bars in Fig. 11 represent the temperature where ice concentrations first exceed 1 cm^{-3} (light bar, where applicable) and the temperature where the saturation ratio drops below 1.0 (heavy bar, where applicable). No model runs with $T_0 \leq -38$°C produce droplets that grow larger than 3 μm before freezing (as also occurs when $W = 10$ cm s^{-1} and $T_0 = -36$°C), and the upper horizontal "half-bar" in these cases represents the temperature at which all droplets of *any* size have frozen or evaporated.

Figure 11 summarizes several general properties of homogeneous ice nucleation from the model.

- At all T_0 warmer than about −30°C, insignificant ice concentrations are produced homogeneously until the air temperature decreases to about −34°C.
- For relatively "warm" initial conditions that allow significant concentrations of droplets to grow larger than 3 μm ($T_0 \geq -34$°C, see Figs. 10b and A2), droplets cannot exist at temperatures below about −35° to −37°C (assuming $W \leq 300$ cm s^{-1}).
- When the air temperature is colder than about −37°C, the liquid phase can only consist of small droplets undetectable by the RICE and FSSP (Figs. 9b and 14). These droplets can only exist over a narrow temperature interval (≤1°C), a consequence of solute effects on the homogeneous ice nucleation rates.
- Unactivated droplets can exist under certain conditions of low T_0 and/or low W, where the peak saturation ratio may remain below 1.0 (as shown by the lack of a heavy bar in some model runs).

5. Summary and conclusions

A 1D numerical model of droplet and ice particle growth and homogeneous ice nucleation has been used to aid in interpretation of aircraft microphysical measurements taken in lenticular wave clouds in the temperature range −29° to −41°C. This study of supercooled liquid water and homogeneous ice nucleation differs from previous studies in several ways: the modeling calculations suggest a complement of instrument signals that provide strong evidence that the homogeneous ice nucleation process was operative; aircraft flight patterns along the wind direction in these clouds allowed measurements to be taken along well-defined parcel trajectories; the particular combination of instrumentation employed, especially the cryogenic hygrometer, provided a unique dataset sufficient to test the model; and numerous penetrations spanning a wide range of temperatures on the same day allowed investigation of the homogeneous ice nucleation process as

a function of temperature under conditions where temporal changes in CCN characteristics or cloud structure were likely not important.

The rationale for proposing that homogeneous ice nucleation is the primary mechanism producing the ice observed in this study is summarized as follows:

1) The absence of ice at temperatures down to about −32°C under conditions of water supersaturation is consistent with the low homogeneous ice nucleation rate expected at this temperature and is suggestive that neither deposition nor immersion nuclei are important to the ice formation process at this and presumably warmer temperatures in these clouds.

2) Insignificant ice concentrations are observed with the FSSP when the relative humidity is substantially ice supersaturated, yet is below that required to cause droplets to form (which could subsequently freeze homogeneously), at temperatures at least as low as −40.7°C. This observation and item 1 suggest that ice formation on deposition nuclei was unimportant at all temperatures sampled in this study.

3) The measurements from various instruments simultaneously show the abrupt transition from droplets to ice crystals in the characteristic manner suggested by the modeling calculations.

4) The measured sizes at which droplets freeze show a temperature dependence consistent with modeling calculations of the homogeneous ice nucleation process. [The relative humidity data are also consistent with the temperature-dependence of the peak saturation ratio expected theoretically from the homogeneous nucleation of solution droplets (Heymsfield and Sabin 1989; Sassen and Dodd 1989).]

5) The temperature dependence of the observed magnitude of change in FSSP-detected particle concentrations across the phase-transition region shows general agreement with that expected from the modeled homogeneous ice nucleation process.

While not entirely conclusive, it would be quite coincidental if some ice nucleation mechanism other than homogeneous nucleation operated in the same temperature range with the same characteristic instrument signatures and approximately the same temperature-dependent rates. Points 1–3 above, as well as other previously cited studies, argue that heterogeneous ice nucleation mechanisms may be unimportant relative to homogeneous ice nucleation at temperatures below −35°C in the upper troposphere, at least for the conditions sampled in this and the other studies.

The complement of instrumentation used in this study was found to be essential to the observational study of supercooled liquid water and homogeneous ice nucleation. Combined interpretation of the FSSP and RICE signals allowed differentiation of liquid-dominated from ice-dominated regions at temperatures above −36°C. The newly developed cryogenic hygrometer provided reliable measurements of relative humidity and provided signals characteristic of homogeneous ice nucleation, which allowed differentiation of liquid from ice at temperatures below −36°C. The following additional conclusions resulted from interpretation of these instrument signals in combination with modeling results.

- Supercooled liquid water was detected at a temperature of −40.7°C, lower than previously documented in situ cloud measurements. There is apparently no fundamental low-temperature physical limit around −40°C to the existence of cloud droplets; modeling results and the measurements suggest that small, unactivated solution droplets merely freeze at smaller sizes and at lower relative humidities as the temperature lowers and can exist for a time following droplet deliquescence as a result of depression of the homogeneous ice nucleation rate by the dissolved solute. Unactivated droplets will freeze homogeneously before reaching liquid saturated conditions at temperatures below about −40°C.
- The temperature-dependent ice nucleation rates employed by the model [Eq. (1) and Fig. 8] appear to fit the observational data well in the temperature range −35° to −38°C. Given the theoretical basis of these rates, it may be reasonable to apply them throughout the −30° to −50°C temperature range considered by the theory.
- Consideration must be given to instrument detection thresholds in interpretation of these and prior measurements in cold clouds. Direct interpretation of only the RICE and FSSP measurements in this study would have implied a total absence of the liquid phase at temperatures colder than about −36°C, as was likely the case in results reported by Sassen and Dodd (1988) and Heymsfield and Sabin (1989).

We have proposed that homogeneous nucleation may play an important role in the *initial* ice formation in cirrus; however, when this ice falls through the updraft and reduces the relative humidity below that at which droplets will form and subsequently freeze homogeneously (conditions also not conducive to ice formation via heterogeneous nucleation), other ice production mechanisms are required to explain the observations of small ice crystals in cirrus.

The theory of homogeneous ice nucleation and the conclusions drawn from this study can be improved through further research in the following areas.

- Given topography and sounding information upwind of wave cloud measurements, dynamical modeling studies would allow a more realistic determination of air motions and reconstruction of microphysical histories in the sampled parcels and hence, quantitative determination of the observed ice nucleation rates as a function of temperature.

- The proposed role of homogeneous ice nucleation in cirrus formation can be investigated with accurately measured profiles of relative humidity coupled with microphysical measurements that include small ice particle sizes.
- Measurements in the upper troposphere are needed to better define the CCN size spectra and chemical composition and to determine their importance to the homogeneous ice nucleation process.

Acknowledgments. We gratefully acknowledge W. (Al) Cooper (NCAR) for the use of his King Air data and for helpful discussion. We also appreciate discussions with Charlie Knight (NCAR) and Don Hagen (University of Missouri at Rolla). The support of the NCAR Research Aviation Facility was instrumental to this study, especially from Ed Brown for coordinating aircraft logistics and Paul Spyers-Duran for developing the airborne cryogenic frost-point hygrometer. This work was supported in part by NASA/FIRE Grant 1-98100-B and by NSF Grant ATM 88-20708 to Don Hagen.

APPENDIX

Modeled Microphysical Characteristics of a Wave Cloud

Specific thermodynamic and microphysical properties of the hypothetical cloud modeled in Fig. 7 (along streamline paths A_S and B_S and along constant level paths A_L and B_L) are shown in Fig. A1, where results from additional intermediate streamlines (not shown in Fig. 7) have been used to provide finer resolution. These paths were chosen for illustration because they span the temperature range where homogeneous ice-nucleation rates significantly affect the liquid phase, and comparisons between them show the dependence of the homogeneous freezing rates on the initial temperature, T_0.

a. Model results along a parcel's trajectory

The parcel streamlines A_S and B_S (bold curves in Fig. A1) show temperature curves that lag the vertical velocity curves by 90° in phase (panel A), as expected in a wave. Droplet growth occurs in both parcels (droplet mean diameter, D_L; panels E and F) until ice nucleation rates become significant, then ice formation (ice concentration, N_I; panels C and D) causes a simultaneous and rapid decline in saturation ratio from liquid-saturated to ice-saturated conditions (panel B). The model shows higher ice concentrations and correspondingly smaller mean ice diameters for the colder parcel along path A_S (panels C and E vs panels D and F) since the temperature-dependence of the ice nucleation rate, J_H, dominates droplet size effects on $J_H VN$ (see Fig. 8), as evident in the rate at which droplets freeze (i.e., the slope of N_I in panel C vs panel D during the rapid freezing stage). Note also that the timing and duration of the freezing event is discernible in the small wiggles in the temperature traces (panel A), primarily the result of latent heat released by the rapid conversion of some 30% of the ambient water vapor to ice mass as the newly frozen ice particles grow quickly in a highly ice-supersaturated environment.

In a general sense, evolution of the microphysical properties of a parcel following a given streamline in a wave cloud can be summarized as follows.

- The CCN deliquesce above 82% relative humidity (if composed of ammonium sulfate), then these solution droplets grow in the updraft. As solute concentrations and temperature decrease, freezing becomes more probable. The largest droplets are the first to experience appreciable homogeneous freezing rates.
- As temperature decreases further the ice nucleation rate, and hence ice concentration, increases. Apart from relatively warm cases where extremely low concentrations of ice particles form, the growing ice rapidly reduces the vapor density, lowering the relative humidity and evaporating the remaining droplets.
- The ice crystals bring the relative humidity to ice saturation, even in strong updrafts, and they continue to grow in the updraft until the wave crest is reached. They sublimate throughout the downdraft, maintaining the parcel at ice saturation until sublimation is complete.

b. Model results along a constant-altitude path

The cross-streamline sampling along the level paths A_L and B_L (light curves in Fig. A1) from the upwind wave trough toward the wave crest (see Fig. 7) provides samples of different parcels that originated (i.e., droplets deliquesced) at successively lower altitudes and warmer temperatures and thus have experienced different microphysical growth histories. Likewise, sampling along a level path from the wave crest to the downwind wave trough provides samples of parcels that attained successively higher altitudes and lower temperatures.

Temperature in a wave varies along a given altitude (panel A) to a degree determined primarily by the upwind lapse rate, the wave amplitude, and the sampling altitude. The temperature changes along A_L and B_L are considerably smaller than those experienced by a parcel but are still of the same "wavelike" form. The horizontal extent of the liquid phase regions (widths of $N_L > 0$ regions in panels C and D) are broader than actually occur in a parcel, a geometrical effect whose magnitude is strongly dependent on the level sampled; thus ice nucleation rates inferred along a constant level (as suggested by the slope of N_I in panels C and D, when ice first forms) are slower than those that actually occur in parcels. Ice particle concentrations and mean diameters display more variability in the horizontal

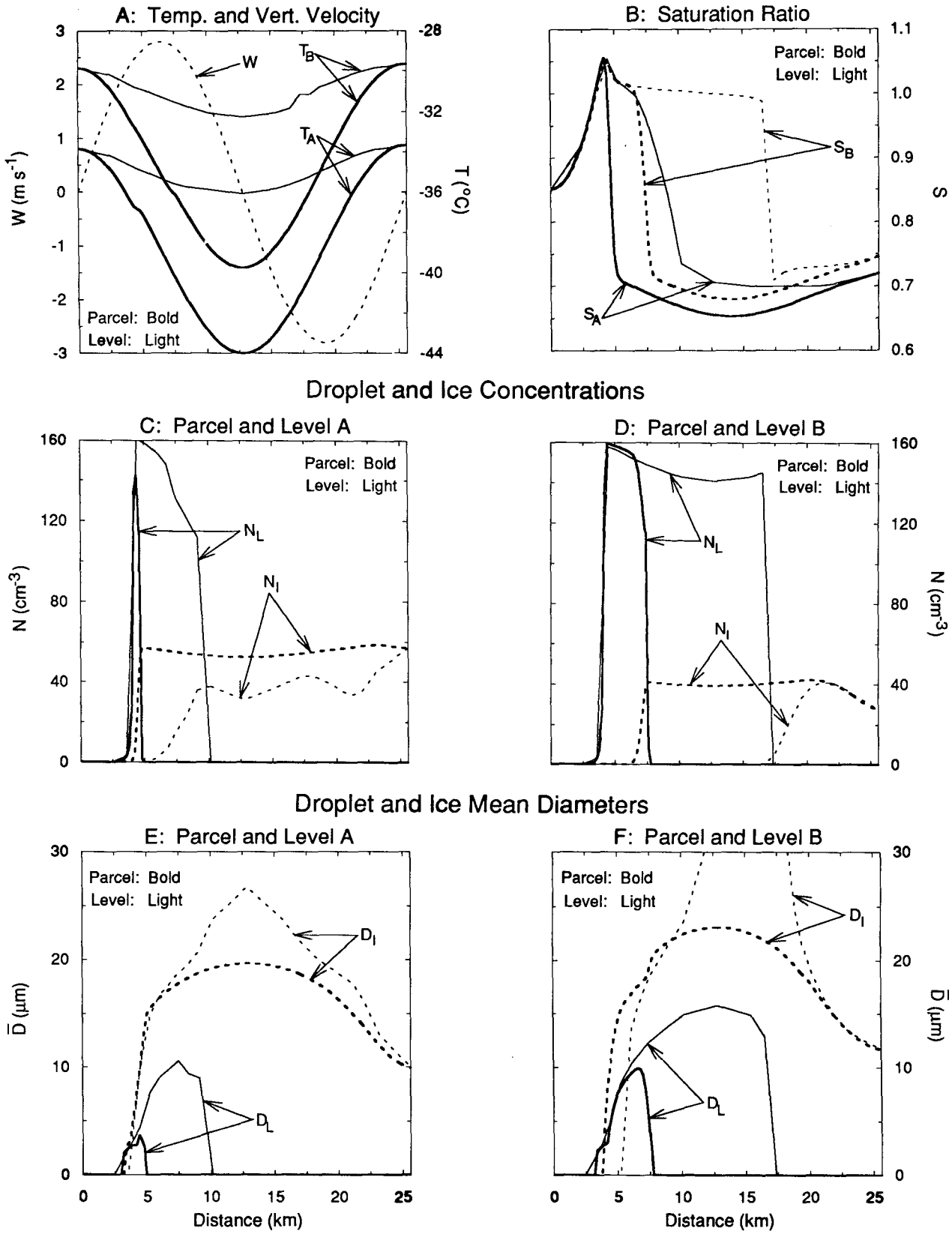

FIG. A1. Microphysical and thermodynamic properties of the wave cloud modeled in Fig. 7 along four paths: two at the constant altitudes labeled A_L and B_L in Fig. 7 and two along the parcel trajectories that begin and end at these levels (labeled A_S and B_S in Fig. 7). Shown are the vertical velocity (W) assumed in the model and temperatures along the two levels and two streamlines (a), the saturation ratio along the four paths (b), the droplet and ice concentration along streamline and level A (c) and along streamline and level B (d), and the droplet and ice mean diameters along streamline and level A (e) and along streamline and level B (f). The CCN mass spectrum ($N = Cs^k$) assumed in the model is $C = 100$ and $k = 0.5$.

than is seen within a parcel (panels C, E, and F) as a result of cross-streamline sampling of parcels that experienced different microphysical growth histories and ice nucleation rates. Note the presence of ice particles of concentrations much lower than the droplets and relatively large in size (panels D and F, distance = 15 km); these result from very low droplet freezing rates at about −32°C. In such cases, where the transition from liquid phase to ice phase occurs downwind of the wave crest (Fig. 7, B_L, distance = 17–20 km), we see that the ice has been transported down from above, having formed at colder temperatures, and thus the actual ice nucleation event has not been detected (as in penetration 5-K, Fig. 6).

c. *Characteristic instrument responses suggested by the model*

The model results shown in Fig. A1 suggest that ice nucleation, as detected by aircraft measurements, might be characterized by "rapid"[6] changes in several aircraft instrumentation signals. The following aircraft instrumentation and associated instrument responses will prove useful in detecting and characterizing ice nucleation events.

- *Cryogenic hygrometer or Lyman-alpha sensor.* An abrupt decrease in implied saturation ratio from liquid saturated to ice saturated conditions indicates a phase change has occurred.
- *RICE probe.* An abrupt decrease to zero (or below) of the derivative of the voltage signal indicates that cloud LWC has dropped below the detection threshold of the instrument. Negative values are the result of sublimation of previously accreted droplets from the sensor.
- *FSSP.* An abrupt change in particle concentration and an increase in particle mean diameter indicates the change in hydrometeor properties expected when droplet freezing occurs. [Note that net droplet plus ice characteristics are detected by the FSSP since the phase cannot be distinguished using this instrument alone.]
- *FSSP, 2D-C, and 2D-P probes.* Sequential signals from these instruments, because they have successively larger size detection thresholds, indicate the growth of droplets and the phase transition and subsequent growth of ice (but only the FSSP is capable of detecting the droplet sizes expected at the low temperatures encountered in this study). In downdrafts, the signals may subsequently disappear from these instruments in the reverse order as ice sublimates.

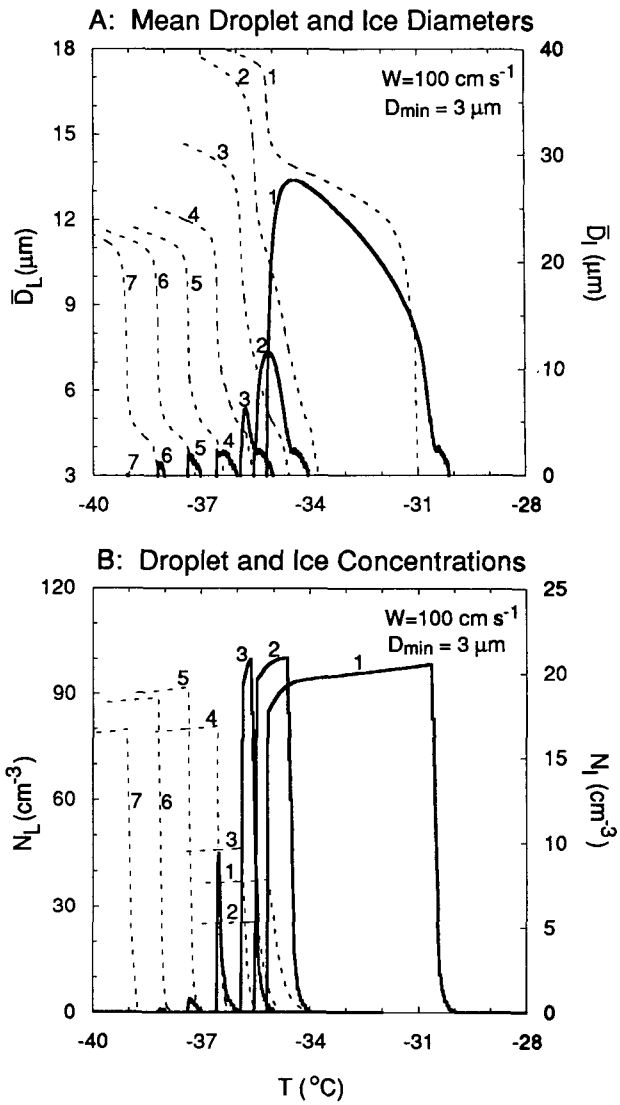

FIG. A2. Curves show the evolution of droplet (solid) and ice (dashed) concentrations and mean diameters for particles larger than 3 μm, where time increases from right to left as temperature decreases in an assumed 100 cm s^{-1} updraft. Model runs are initialized at 85% relative humidity and use different initial temperatures (T_0) of −28°C (labeled 1), −32°C (2), −33°C (3), −34°C (4), −35°C (5), −36°C (6), and −37°C (7). The power-law form of the assumed CCN mass spectrum is given by constants C and k of 62 and 0.5, respectively, which produces a total CCN concentration of about 100 cm^{-3}.

- *Temperature probe.* Relative warming, as determined by a temperature gradient that differs from immediately adjacent regions, may indicate the release of latent heat accompanying rapid ice growth immediately after ice nucleation. This signal may be indistinguishable from instrument noise and small changes in aircraft altitude.
- *Probe detection threshold considerations.* The characteristic freezing signals described above for the

[6] The term "rapid" is used to indicate an event that occurs in a time period of one or a few seconds of aircraft flight time, where one-second aircraft measurements correspond to 6–10 s of parcel transport or 90–250 m in the horizontal, for an aircraft flight speed of 150 m s^{-1} and typical horizontal windspeeds of 15–25 m s^{-1}.

RICE and FSSP may be undetectable below about −36°C as a result of instrument-detection thresholds. The RICE LWC detection threshold of about 0.002 g m^{-3} corresponds to a droplet size detection threshold of about 3 μm if the droplet concentration is 100 cm^{-3} (assuming 100% collection efficiency), approximately the same as the nominal size-detection threshold of the FSSP. The temperature that corresponds to the RICE and FSSP size detection thresholds is estimated from the model results shown in Fig. A2. This series of model runs shows *detectable* (defined here as ≥ 3 μm) droplet and ice concentrations and mean diameters in parcels that lift from successively lower initial temperatures (T_0) at a constant velocity of 100 cm s^{-1}. (The existence of droplets larger than 3 μm at temperatures ≤ -37°C results from the few largest aerosols in the assumed CCN mass spectrum.) Droplet sizes and LWC decrease rapidly in the vicinity of −36°C as a result of the strong temperature dependence of J_H; thus droplets become undetectable by the RICE and FSSP below about −36°C.

REFERENCES

Baumgardner, D., and M. Spowart, 1990: Evaluation of the forward-scattering probe. Part III: Time response and laser inhomogeneity limitations. *J. Atmos. Oceanic Technol.*, **7**, 666–672.

Buck, A. L., 1976: The variable-path Lyman-alpha hygrometer and its operating characteristics. *Bull. Amer. Meteor. Soc.*, **57**, 1113–1118.

Byers, H. R., 1965: *Elements of Cloud Physics.* The University of Chicago Press, 191 pp.

Cox, S. K., D. S. McDougal, D. A. Randall, and R. A. Schiffer, 1987: FIRE—The First ISCCP Regional Experiment. *Bull. Amer. Meteor. Soc.*, **88**, 114–118.

Day, J. A., 1958: On the freezing of three to nine micron water droplets. *J. Meteor.*, **15**, 226–228.

DeMott, P. J., and D. C. Rogers, 1990: Freezing nucleation rates of dilute solution droplets measured between −30°C and −40°C in laboratory simulations of natural clouds. *J. Atmos. Sci.*, **47**, 1056–1064.

Eadie, W. J., 1971: A molecular theory of the homogeneous nucleation of ice from supercooled water. Ph.D. dissertation, University of Chicago Cloud Physics Laboratory, Chicago, Illinois, Tech. Note 40, 117 pp. [NTIS PB201625.]

Gardiner, B. A., and J. Hallett, 1985: Degradation of in-cloud forward-scattering spectrometer probe measurements in the presence of ice particles. *J. Atmos. Oceanic Technol.*, **2**, 171–180.

Heymsfield, A. J., 1977: Precipitation development in stratiform ice clouds: A microphysical and dynamical study. *J. Atmos. Sci.*, **34**, 367–381.

Hobbs, P. V., and A. L. Rangno, 1985: Ice particle concentrations in clouds. *J. Atmos. Sci.*, **42**, 2523–2549.

——, and C. M. R. Platt, 1984: A parameterization of the particle size spectrum of ice clouds in terms of the ambient temperature and ice water content. *J. Atmos. Sci.*, **41**, 846–855.

——, and L. M. Miloshevich, 1989: Evaluation of liquid water measuring instruments in cold clouds sampled during FIRE. *J. Atmos. Oceanic Technol.*, **6**, 378–388.

——, and R. M. Sabin, 1989: Cirrus crystal nucleation by homogeneous freezing of solution droplets. *J. Atmos. Sci.*, **46**, 2252–2264.

——, L. M. Miloshevich, A. Slingo, K. Sassen, and D. Starr, 1991: An observational and theoretical study of highly supercooled altocumulus. *J. Atmos. Sci.*, **48**, 923–945.

Hosler, C. L., and G. R. Spalding, 1955: An experimental study of the effects of aerosols of a number of pure chemicals on the freezing characteristics of supercooled liquid drops. Final Report. Air Force Cambridge Research Center, Contract AF 19(604)-140. [Available from Dr. Charles Hosler, 617 Walker Building, The Pennsylvania State University, University Park, Pennsylvania 16802.]

Ramanathan, V., and W. Collins, 1991: Thermodynamic regulation of ocean warming by cirrus clouds deduced from the 1987 El Niño. *Nature*, **351**, 27–32.

Raschke, E., 1988: The international satellite cloud climatology project, ISCCP, and its European regional experiment ICE (International Cirrus Experiment). *Atmos. Res.*, **21**, 191–201.

Sassen, K., and G. C. Dodd, 1988: Homogeneous nucleation rate for highly supercooled cirrus cloud droplets. *J. Atmos. Sci.*, **45**, 1357–1369.

——, and ——, 1989: Haze particle nucleation simulations in cirrus clouds, and applications for numerical modeling and lidar studies. *J. Atmos. Sci.*, **46**, 3005–3014.

Schaefer, V. J., 1962: Condensed water in the free atmosphere in air colder than −40°C. *J. Appl. Meteor.*, **1**, 481–488.

Simpson, R. H., 1963: Liquid water in squall lines and hurricanes at temperatures lower than −40°C. *Mon. Wea. Rev.*, **91**, 687–693.

Smith, W. L., 1990: The 27–28 October 1986 FIRE IFO cirrus case study: In situ observations of radiation and dynamic properties of a cirrus cloud layer. *Mon. Wea. Rev.*, **118**, 2389–2401.

Spyers-Duran, P., 1991: An airborne cryogenic frost-point hygrometer. *Proc. Seventh Symp. on Meteorological Observations and Instrumentation,* New Orleans, Amer. Meteor. Soc., 303–306.

——, and A. Schanot, 1987: Airborne intercomparison of three hygrometers. *Proc. Sixth Symp. on Meteorological Observations and Instrumentation,* New Orleans, Amer. Meteor. Soc., 209–212.

Stephens, G. L., S. Tsay, P. W. Stackhouse, Jr., and P. Flatau, 1990: The relevance of the microphysical and radiative properties of cirrus clouds to climate and climatic feedback. *J. Atmos. Sci.*, **47**, 1742–1753.

Wielicki, B. A., J. T. Suttles, A. J. Heymsfield, R. M. Welch, J. D. Spinhirne, M. Wu, D. Starr, L. Parker, and R. F. Arduini, 1990: The 27–28 October 1986 FIRE IFO cirrus case study: Comparison of radiative transfer theory with observations by satellite and aircraft. *Mon. Wea. Rev.*, **118**, 2356–2376.